Improving PSK performance in snapping shrimp noise with rotated constellations

Ahmed Mahmood*, Mandar Chitre*†, Marc A. Armand*
*Dept. of Electrical and Computer Engineering, National University of Singapore, Singapore 117576
†Acoustic Research Laborotary, National University of Singapore, Singapore 119227
{ahmed.mahmood, mandar, eleama}@nus.edu.sg

ABSTRACT

Snapping shrimp are small marine animals that are typically found in coastal regions with coral reefs. These crustaceans live in droves and are the dominant source of high-frequency ambient noise in their habitat. The noise generated by the shrimp is impulsive and is detrimental to the performance of sonar and underwater communication systems. In this paper we use heavy-tailed symmetric α-stable (SαS) distributions to model snapping shrimp noise. In conventional digital communication systems, most processing is done at the baseband level. We investigate the characteristics of complex baseband noise derived from passband additive white symmetric α-stable noise (AWSαSN) using linear passband-to-baseband converters. The resulting baseband noise distributions, although symmetric, are generally anisotropic with dependent components. Further still, the geometric structure of the anisotropy may be controlled by varying certain system parameters. We exploit this structure to enhance error performance for the binary and quadrature phase shift keying (BPSK/QPSK) schemes by rotating constellations.

Categories and Subject Descriptors

C.2.0 [**Computer-Communication Networks**]: General—*Data communications*; E.4 [**Coding and Information Theory**]: Formal models of communication; I.6.6 [**Simulation and Modeling**]: Simulation Output Analysis

1. INTRODUCTION

Snapping shrimp are small crustaceans that live in large droves typically inhabiting coral reefs in warm shallow waters. A unique characteristic of this species is their ability to produce sharp snaps by cavitating bubbles [16]. These snaps have been recorded to be as high as 189 dB re 1 μPa @ 1 m and are loud enough to stun or even kill small prey [2]. In large groups, the cumulative effect of these snaps creates a crackling effect which is detrimental for sonar and underwater communication systems. The noise produced by the shrimp is impulsive and non-Gaussian in nature [3, 9].

WUWNet'12, Nov. 5 - 6, 2012 Los Angeles, California, USA.

Gaussian noise models are conventionally used to simulate practical communication systems. This approximation is motivated by the central limit theorem (CLT) [13, 14]. However, Gaussian distributions fail to adequately model channels corrupted by *impulsive noise* [11, 15]. Models based on symmetric α-stable (SαS) distributions are known to approximate practical impulsive noise very well [11]. The zero-mean Gaussian distribution is a member of the SαS family. With the exception of the Gaussian case, all SαS distributions are heavy-tailed, allowing modeling of impulses in a more effective manner. The motivation of using SαS models stems from the generalized central limit theorem (GCLT), which in essence is the CLT with the power constraint removed [11, 12, 15].

Though an SαS model provides a good solution for simulating impulsive noise, several issues arise with its use. With the exception of the Gaussian and Cauchy cases, the probability density function (pdf) of an SαS random variable does not exist in closed form. One approach to circumvent this problem is to work with the characteristic function (cf) of a random variable which is the Fourier transform of its pdf. Fortunately, the cf of an SαS random variable exists in closed form [11, 15]. Another obstacle associated with non-Gaussian SαS random variables is the non-existence of second order moments. In digital communications, error performance is typically analyzed by plotting against the signal-to-noise ratio (SNR). In the literature, suitable SNR measures have been proposed to bypass the issue that conventional SNR calculation imposes on SαS noise channels [7, 10].

Optimal and near-optimal filters, smoothers and predictors have been designed for noise scenarios modelled under the SαS framework [1]. The *myriad filter* and its variants are examples of techniques that display optimality properties in SαS noise [4, 5, 6, 8]. Though superior in enhancing noise error performance, these schemes introduce nonlinearities in the received signal [1]. Practical communication channels generally consist of several physical impairments besides additive noise. Applying a nonlinear technique such as the myriad filter would trigger a redesign of those elements in a communication system that deal with other channel effects. By restricting our work to linear techniques, our ideas can be easily accommodated within any existing practical system. The work presented in this paper highlights characteristics unique to impulsive noise baseband channels. These insights provide an essential platform for future designing of robust and rate-efficient digital communication systems operating in impulsive noise.

We illustrate key ideas using the Cauchy distribution, which is a specific member of the SαS family with very heavy tails and a closed form pdf. The intuition gained from studying the case of Cauchy noise is also applicable to other heavy-tailed SαS cases. In Section 2 we summarize the properties of complex baseband noise derived from passband additive white SαS noise (AWSαSN). The baseband noise is generally anisotropic with star-like equiprobable density surfaces [10]. Further still, one may achieve different configurations of the bivariate pdf of a baseband noise sample by tuning certain system parameters. Motivated by these facts, in Section 3, we propose efficient placement of signal points on constellation diagrams for the binary phase shift keying (BPSK) and quadrature phase shift keying modulation (QPSK) schemes with emphasis on the case with independent real and imaginary components. In Section 4, we discuss how the suggested solution may be practically implemented.

2. COMPLEX BASEBAND SαS NOISE

We summarize important aspects of SαS variables/vectors, the AWSαSN channel and complex baseband noise derived from passband AWSαSN.

2.1 SαS Variables

A stable random variable X is symmetric if its pdf $f_X(x)$ is an even function of x, i.e., $f_X(x) = f_X(-x)$. The cf of X is then of the following form [15]:

$$\Phi_X(\theta) = \exp\left(-\delta^\alpha |\theta|^\alpha\right) \tag{1}$$

where $\delta \in (0, +\infty)$ is the *scale parameter* of the distribution. The *characteristic exponent* 'α' lies in $(0, 2]$ and quantifies the heaviness in the tails of the distribution. The tails consistently become heavier as $\alpha \to 0$. For $\alpha = 2$ and $\alpha = 1$ the distribution is that of a Gaussian and a Cauchy random variable, respectively [15]. Practical estimates of α for snapping shrimp noise typically lie within $1.5 \sim 1.9$ [3].

The fact that $\Phi_X(0) = 1$ in (1) ensures that $f_X(x)$ is a valid pdf. Further still, as $\Phi_X(\theta)$ is real and an even function of the frequency domain variable θ, we conclude from the properties of the Fourier transform that $f_X(x)$ is real and symmetric about $X = 0$. For the Gaussian case, the cf in (1) corresponds to $\mathcal{N}(0, 2\delta^2)$, i.e., the zero-mean Gaussian distribution with variance $2\delta^2$. For the Cauchy case, the pdf corresponding to the cf in (1) is

$$f_X(x) = \frac{\delta}{\pi(x^2 + \delta^2)} \tag{2}$$

The concept of symmetry may be extended to the multivariate α-stable case, i.e., if there exists an N-dimensional SαS random vector $\vec{X}$ with density function $f_{\vec{X}}(\vec{x})$, then $f_{\vec{X}}(\vec{x}) = f_{\vec{X}}(-\vec{x})$. This implies that the cf of $\vec{X}$ is real and an even function of the N-dimensional vector $\vec{\theta}$, i.e., $\Phi_{\vec{X}}(\vec{\theta}) = \Phi^*_{\vec{X}}(\vec{\theta}) = \Phi_{\vec{X}}(-\vec{\theta})$. Here, $\vec{\theta}$ is a column vector with elements $\theta_i \; \forall \; i \in \{1, 2, \ldots, N\}$, where θ_i is the frequency domain variable corresponding to the i^{th} element in $\vec{X}$.

2.2 The AWSαSN Channel

If there exists an SαS noise *process* such that all samples $X(n)$ are IID, where n is the discrete-time index, then the

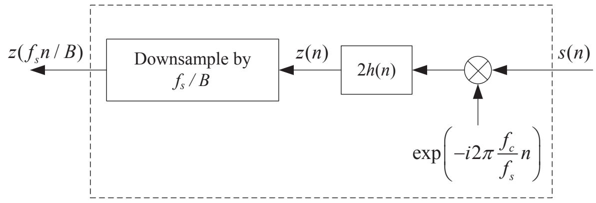

Figure 1: The passband-to-baseband conversion schematic.

joint-cf of any N samples may be evaluated using (1):

$$\begin{aligned}\Phi_{\vec{X}_N}(\vec{\theta}) &= \prod_{i=1}^{N} \Phi_{X(n)}(\theta_i) \\ &= \prod_{i=1}^{N} \exp\left(-\delta^\alpha |\theta_i|^\alpha\right) \\ &= \exp\left(-\delta^\alpha \sum_{i=1}^{N} |\theta_i|^\alpha\right)\end{aligned} \tag{3}$$

where $\vec{X}_N$ is an N-dimensional column vector whose elements $X_i \; \forall \; i \in \{1, 2, \ldots, N\}$ consist of any combination of N different samples of the noise process. The joint-cf in (3) is multivariate SαS. If the noise process $X(n)$ is additive, it is called AWSαSN. For $\alpha = 2$, the cf in (3) reduces to that of additive white Gaussian noise (AWGN). As the second order moments of non-Gaussian α-stable variables do not exist, the power spectral density (psd) of noise models based on this family will always be infinite. The term 'white' then highlights the independence of time samples rather than a flat psd.

2.3 Baseband SαS Noise

The relationship of a passband signal $s(n)$ with its *upsampled* baseband form $z(n)$ is given by

$$s(n) = \Re\left\{z(n)\exp\left(i2\pi\frac{f_c}{f_s}n\right)\right\} \tag{4}$$

where f_c and f_s are the carrier and passband sampling frequencies, respectively. Conversion from passband-to-baseband is accomplished by shifting the spectrum of $s(n)$ by f_c/f_s and passing the result through a low-pass filter. The output is then downsampled by f_s/B to generate the baseband signal $z(f_s n/B)$. The passband-to-baseband conversion block is depicted in Fig. 1. If $s(n)$ comprises of pure AWSαSN samples, the bivariate cf of any $z(n)$ is [10]:

$$\Phi_{\vec{Z}}(\vec{\theta}) = \exp\left(-\sum_{k=0}^{M-1}\left|2h^2(k)\vec{\theta}^t\mathbf{R}(n-k)\vec{\theta}\right|^{\alpha/2}\right) \tag{5}$$

where $h(n)$ is the impulse response of the M-tap low-pass FIR filter with normalized cutoff B/f_s and $\vec{Z}$ is a 2-dimensional column vector whose elements are the real and imaginary parts of $z(n)$. Also,

$$\mathbf{R}(n) = 2\delta^2\begin{bmatrix}\cos^2(2\pi\frac{f_c}{f_s}n) & -\frac{1}{2}\sin(4\pi\frac{f_c}{f_s}n) \\ -\frac{1}{2}\sin(4\pi\frac{f_c}{f_s}n) & \sin^2(2\pi\frac{f_c}{f_s}n)\end{bmatrix} \tag{6}$$

where δ is the scale parameter of the passband noise. Assuming the Nyquist criterion $f_s > 2f_c + B$ is met, the following observations are drawn from (5):

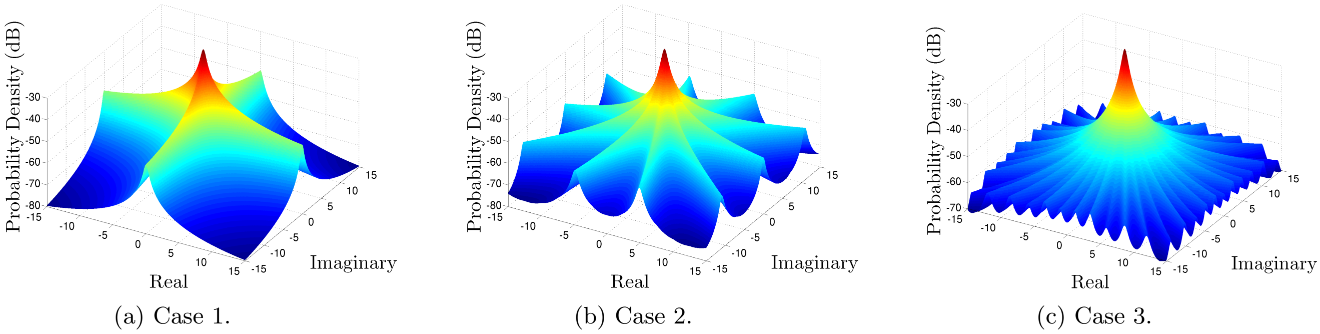

Figure 2: Probability density functions of complex baseband SαS noise for the Cauchy case ($\alpha = 1$) under the assumption of white passband noise. The parameters that generate each of these plots are summarized in Table 1.

Table 1: Parameter settings for generating the density functions in Fig. 2.

Case	f_c	f_s	Number of Tails	B	δ
1.	4	16	4	1	1
2.	4	20	10	1	1
3.	4	21	42	1	1

- $\Phi_{\vec{Z}}(\vec{\theta})$ is real and symmetric about $\vec{\theta} = 0$, proving that every complex sample $z(n)$ is bivariate SαS.
- The baseband samples $z(f_s/Bn)$ are mutually independent if $M \leq \lfloor f_s/B \rfloor$. This condition ensures that no passband noise sample $s(n)$ is involved in creating any more than one baseband sample. As all $s(n)$ are mutually independent, the baseband samples will be independent as well.
- For M large enough to induce an effective low-pass filtering effect, $\Phi_{\vec{Z}}(\vec{\theta})$ does not vary with time. This implies that the statistics of individual baseband noise samples are identical.

For the Gaussian case, (5) decomposes into the product of its marginals, implying that the real and imaginary components of any complex baseband noise sample are independent [10]. It is also well known that the corresponding bivariate distribution is isotropic [14]. These results cannot be extended as a general rule to all SαS cases. For baseband noise derived from non-Gaussian AWSαSN, the statistical properties depend entirely on the system parameters f_s, f_c and B. By altering these parameters one may attain different bivariate pdf configurations. The heavy-tailed phenomenon associated with SαS distributions will be observed in the baseband noise, but only in specific directions in the complex plane.

We present baseband noise pdfs for the Cauchy case in Fig. 2. The system parameters used to generate these plots are summarized in Table 1. The order of the filter was fixed at 800 for each case. It is observed that most of the probability is directed along a certain number of 'tails' in the complex plane. To be precise, the number of tails is given by

$$\left.\begin{array}{ll} \frac{f_s}{\gcd(f_c, f_s)} & \text{if } f_s \text{ is an even multiple of } f_c \\ \frac{2f_s}{\gcd(f_c, f_s)} & \text{otherwise} \end{array}\right\} \tag{7}$$

where gcd denotes the greatest common divisor. The angular distance between adjacent tails is constant. Results from Cauchy noise may be intuitively extended to other heavy-tailed SαS cases ($\alpha \neq 2$).

To ensure independence of the real and imaginary components of all baseband noise samples, f_s has to be set to $4f_c$ [10]. This setting allows $\mathbf{R}(n)$ to degenerate into a diagonal matrix, allowing the joint-cf in (5) to factor into a product of its marginal cfs, thus implying independence. From (7), we see that the number of tails for the independent case is four, thus making it non-isotropic. Hence, for independent components, the bivariate distribution of any complex baseband sample is not isotropic with the only exception being the Gaussian case. It may also be observed that as the number of tails tends to infinity, the distribution converges to an isotropic one.

2.4 The Case of Independent Components

The case of baseband samples with independent components is of special interest. This is due to the fact that for a given α, the probability of error associated with this case will be lower in comparison to all possible dependent cases. To support this statement we propose the following argument: The joint-entropy of the real and imaginary components of any baseband noise sample may be written as

$$H(Z_R, Z_I) = H(Z_R) + H(Z_I) - I(Z_R; Z_I) \tag{8}$$

where $H(Z_R)$ and $H(Z_I)$ are the entropies of the I and Q components, respectively and $I(Z_R; Z_I)$ is the mutual information between them. It is assumed that there is no loss of information (unique mapping) in the passband-to-baseband conversion process. Thus, $H(Z_R, Z_I)$ will always be the same, irrespective of any combination of system parameters. For the independent case the mutual information will be zero, hence implying that the sum $H(Z_R) + H(Z_I)$ will be less than the corresponding sum in each and every one of the dependent cases. Further still, $H(Z_R)$ and $H(Z_I)$ will be identical for the independent case. Conventionally, the real and imaginary components are separately decoded. Due to the relatively lower entropies of the I and

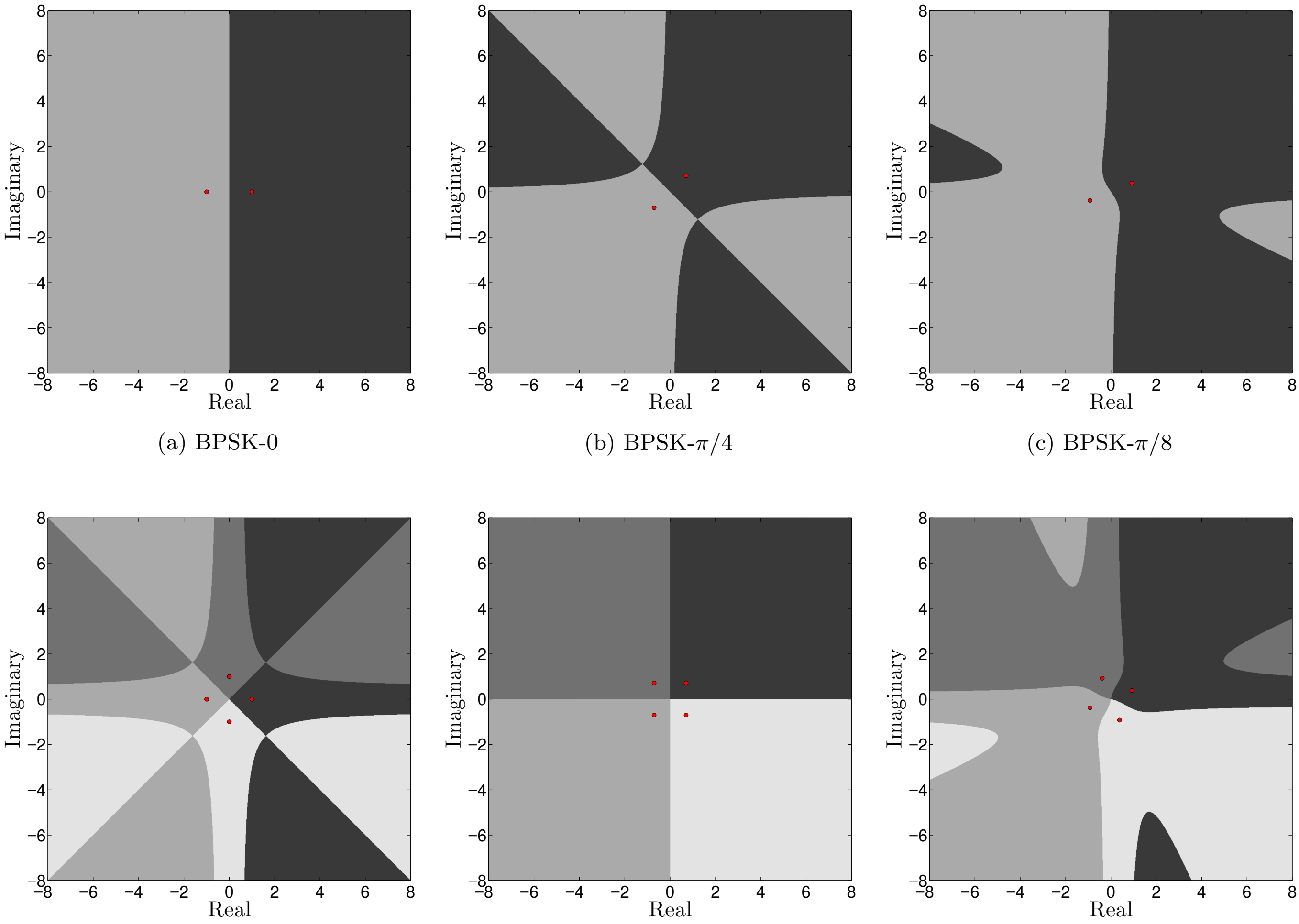

(a) BPSK-0 (b) BPSK-$\pi/4$ (c) BPSK-$\pi/8$

(d) QPSK-0 (e) QPSK-$\pi/4$ (f) QPSK-$\pi/8$

Figure 3: Optimum decision regions for the Cauchy case ($\alpha = 1$) with independent baseband noise components for various rotated versions of BPSK and QPSK.

Q components, the probability of error will be lower for the independent case.

For the remainder of this paper we focus on the case with independent baseband components as it delivers the best error performance using linear decoders. The pdf in Fig. 2a corresponds to baseband Cauchy noise with independent components.

If the components of the resulting baseband noise are independent, (5) may be factored into a product of its marginal distributions

$$\Phi_{\vec{Z}}(\vec{\theta}) = \Phi_{Z_R}(\theta_1)\Phi_{Z_I}(\theta_2) \tag{9}$$

where

$$\Phi_{Z_R}(\theta) = \exp\Bigg(-\underbrace{\sum_{k=0}^{M-1}\left|2h(k)\cos\left(\frac{\pi}{2}(n-k)\right)\delta\right|^{\alpha}}_{\delta_b^{\alpha}}|\theta|^{\alpha}\Bigg) \tag{10}$$

$$\Phi_{Z_I}(\theta) = \exp\Bigg(-\underbrace{\sum_{k=0}^{M-1}\left|2h(k)\sin\left(\frac{\pi}{2}(n-k)\right)\delta\right|^{\alpha}}_{\delta_b^{\alpha}}|\theta|^{\alpha}\Bigg) \tag{11}$$

Both Z_R and Z_I are individually and identically SαS with scale parameter δ_b [10].

3. EFFECTIVE SIGNAL CONSTELLATIONS

Decision regions optimized for the well known Gaussian case (isotropic) will not be optimal for non-Gaussian SαS noise with independent components [10]. We limit our discussion to decision regions evaluated for various rotated BPSK and QPSK schemes. By a rotated version, we imply that all constellation points are equally rotated around the origin by a certain angle. We denote these schemes by BPSK-ϕ and QPSK-ϕ where ϕ is the angle (in radians) of the signal point in the first quadrant from the positive real axis.

In the Gaussian case, the symbol error rate (SER) is independent of ϕ as the baseband noise is isotropic. Further still, for any given ϕ, the decision regions do not vary with the signal-to-noise ratio (SNR). These results cannot be extended to the general SαS case. This raises the question of the existence of an optimal value for ϕ that ensures minimum SER. Further still, would this value of ϕ depend on the SNR?

For $\alpha < 2$, the cfs in (10) and (11) correspond to heavy-tailed univariate SαS distributions. For the Cauchy case, the pdfs of the real and imaginary components will each be of the form

$$f_Z(z) = \frac{\delta_b}{\pi(z^2 + \delta_b^2)} \quad (12)$$

In Fig. 3 we present the optimum decision regions of a few rotated BPSK and QPSK schemes with complex baseband Cauchy noise with independent components. The regions were evaluated using the maximum likelihood (ML) detection rule for $\delta_b = 1$, with all constellation points lying on the unit circle. We note that the regions in Figs. 3a and 3e are the same as the isotropic case for the same ϕ. These regions do not vary with SNR. We prove this for the BPSK-0 scheme: Denoting the signal points by $x_0 = 1$ and $x_1 = -1$, the ML decision for each point in the complex plane is evaluated by

$$\arg\max_{x \in \{x_0, x_1\}} f_Z(z_R - x) = \arg\min_{x \in \{x_0, x_1\}} (z_R - x)^2$$
$$= \begin{cases} x_0 & \text{if } z_R \geq 0 \\ x_1 & \text{if } z_R < 0 \end{cases} \quad (13)$$

where z_R is the real component of a complex baseband noise sample. This reasoning may be extended to the QPSK-$\pi/4$ scheme. However, for all other values of ϕ, the ML decision regions will depend on the SNR.

As a significant probability lies along the tails, one would want to rotate the constellation in such a way that there is minimal tail overlap. Due to symmetry of the bivariate pdf, one would want to direct the tails away from the signal points. This will ensure that the tails do not point towards each other, hence avoiding complete tail overlap. This makes BPSK-0, QPSK-0 and QPSK-$\pi/4$ undesirable.

For BPSK, an angle of $\pi/4$ minimizes the error rate, since this angle achieves the minimum tail overlap. This is shown using the following approximation: First we note that due to the rotational symmetry of the noise pdf and the placement of constellation points, the optimum angle would lie within $[0, \pi/4]$. Let the sent symbol be $x = x_R + ix_I$ where x_R and x_I are its real and imaginary components, respectively. Denoting P_ϕ as the set of all coordinate points (z_R, z_I) in the complex plane that fall in the incorrect decision region given x is sent, the optimum angle is

$$\phi_{\text{opt}} = \arg\min_{\phi \in [0,\pi/4]} \sum_{(z_R, z_I) \in P_\phi} f_Z(z_R - x_R)\, f_Z(z_I - x_I) \quad (14)$$

The expression in (14) may be numerically evaluated over a finite set of coordinate points that lie in P_ϕ to give a suitable approximation of ϕ_{opt}. Using this approach, the optimum angle was evaluated to be $\pi/4$.

For the QPSK case, the decision regions are more complicated. Like BPSK, the optimum angle should lie within $[0, \pi/4]$ for precisely the same reasons. From the findings in BPSK, one would want to direct the tails towards the gaps between the constellation points. Intuitively, for high SNR,

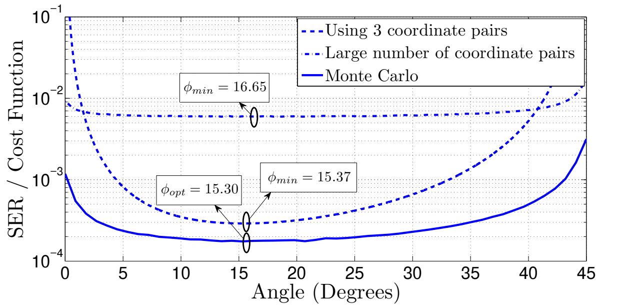

Figure 4: Symbol Error Rate / Cost Function vs. The Rotation angle for the Cauchy case with independent noise components.

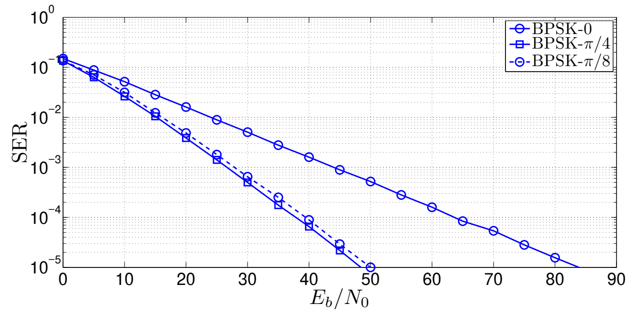

Figure 5: Symbol Error Rate vs. E_b/N_0 for the Cauchy case with independent components for various BPSK schemes.

one would expect the tails to align a little towards the opposite constellation point as it is further away in comparison to the adjacent points, i.e., $\phi_{\text{opt}} < \pi/8$. On the other hand δ_b is high at low SNR. This results in 'thickening' of the tails. The small relative distance between the adjacent and opposite points becomes inconsequential allowing the tails to bisect the spaces between the points equally, i.e., the QPSK-$\pi/8$ case would be optimal. As the SNR increases, it was numerically determined that ϕ_{opt} converges to 15.3 degrees.

Computing ϕ_{opt} in (14) can be computationally intensive. To achieve accurate results one needs to select coordinate pairs over a large range to compensate for the heavy-tails. By choosing a small number of specific points, it is possible to approximate ϕ_{opt} with significantly less computational complexity (albeit with more estimation error). For BPSK the coordinate set was chosen to consist only of the opposite constellation point. For QPSK, the selected coordinates were both the adjacent and the opposite constellation points. This method gives good approximation at high SNR values.

Fig. 4 depicts how the cost function in (14) varies with ϕ for QPSK. The dash-dot curve was generated using a large finite set of equally spaced coordinate points, while the dashed line was generated using the opposite and the adjacent constellation points. The value for ϕ at which both these curves attain their minimum have been highlighted and denoted by $\phi_{\min}$. The solid line depicts the variation of the SER against ϕ and was evaluated using a Monte Carlo simulation for at least 10000 errors. All curves were generated at an SNR per bit (E_b/N_0)[1] of 40 dB. This SNR is of practical interest as

[1]In the Gaussian case, the SNR per bit (E_b/N_0) is equal

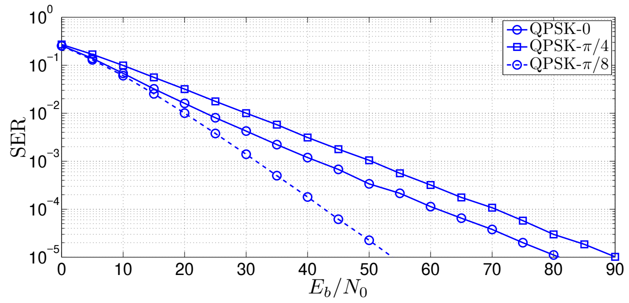

Figure 6: Symbol Error Rate vs. E_b/N_0 for the Cauchy case with independent components for various QPSK schemes.

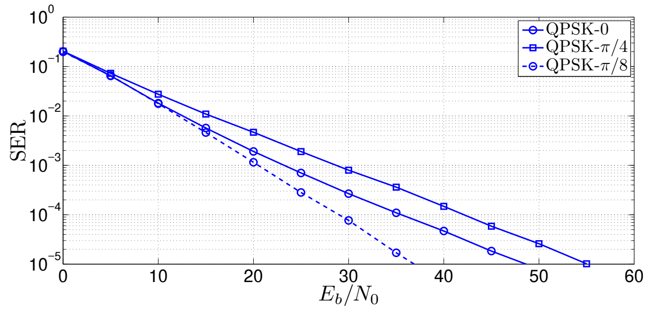

Figure 7: Symbol Error Rate vs. E_b/N_0 for the $\alpha = 1.5$ case with independent components for various QPSK schemes.

the corresponding SER is approximately 10^{-4} for ϕ equal or close to $\phi_{\rm opt}$. It is observed that the SER is approximately the same for a certain range of ϕ, i.e., between 10 to 30 degrees approximately. Any ϕ chosen from this interval would give good results. We see that $\phi_{\rm opt}$ – the angle at which the solid line is at its minimum – is closely approached by the approximation $\phi_{\rm min}$ offered by the other curves.

To appreciate the substantial increase in error performance due to constellation point placement, we have plotted the uncoded SER against E_b/N_0 for various ϕ in Fig. 5 for BPSK and Fig. 6 for QPSK, for the Cauchy case with independent components using ML detection. The gain between the worst and optimum cases for both schemes is over 35dB at an error rate of 10^{-5}. Estimates for α within the AWSαSN framework for practical underwater ambient noise have been recorded to be as low as $\alpha = 1.5$. In Fig. 7 we present the uncoded SER for QPSK in an AWSαSN channel with $\alpha = 1.5$ with independent baseband noise components. It is observed that the trends encountered in the Cauchy case extend to this case as well. All curves were calculated for a minimum of 3000 errors for high SER ($> 10^{-3}$) and a minimum of 1000 errors for low SER ($< 10^{-3}$).

4. PRACTICAL CONSIDERATIONS

From a practical perspective, the rotation of a constellation map can be accomplished at the receiver *without* actually transmitting the rotated constellation symbols themselves. This of course is only of interest if the baseband noise components are anisotropic. We propose a mechanism that not only incorporates constellation rotation at the receiver, but also generates baseband noise with independent components assuming passband AWSαSN.

Let us assume that a single-carrier scheme is to be implemented over an impulsive noise channel and the transmitted symbols are chosen from the QPSK-ϕ_1 configuration. Also, let the optimal constellation map for this particular realization of the channel be QPSK-$\phi_{\rm opt}$. Each symbol in QPSK-ϕ_1 can be mapped on to a unique point in QPSK-$\phi_{\rm opt}$ by multiplying it with $\exp(i\Delta\phi)$ where $\Delta\phi = \phi_{\rm opt} - \phi_1$. This mapping corresponds to a rotation of the constellation points in QPSK-ϕ_1 to attain QPSK-$\phi_{\rm opt}$.

to $d^2/(4m\delta_b^2)$, where d^2 is the average power of the constellation points lying in the complex plane, δ_b^2 is the scale parameter of the real and imaginary baseband noise components and m is the number of information bits per symbol. We extend this definition of E_b/N_0 to the Cauchy case.

The relationship between the transmitted passband signal and its baseband counterpart is given by

$$s(t) = \Re\{z(t)\exp(i2\pi f_c t)\} \tag{15}$$

Note that (15) is the continuous-time version of (4). As $z(t)$ is the baseband signal corresponding to (a sequence of) symbols in QPSK-ϕ_1, $z(t)\exp(i\Delta\phi)$ will be the baseband signal if the symbols are chosen from QPSK-$\phi_{\rm opt}$. We can rewrite (15) as

$$s(t) = \Re\big\{z(t)\exp(i\Delta\phi)\underbrace{\exp\big(i(2\pi f_c t - \Delta\phi)\big)}_{\text{carrier}}\big\} \tag{16}$$

On comparing (15) with (16), it is observed that given $s(t)$, $z(t)\exp(i\Delta\phi)$ can be acquired if the carrier (or clock) at the receiver lags that of the transmitter by $\Delta\phi$. For example, if QPSK-$\pi/4$ is the transmitted constellation and $\phi_{\rm opt} = \pi/8$, the QPSK-$\pi/8$ constellation map can be generated by letting the receiver clock lag the transmitter clock by $\Delta\phi = -\pi/8$.

Though we have concocted a mechanism that rotates the constellation at the receiver, independence of baseband noise components is only ensured if the received signal $s(t)$ is sampled at

$$t = \frac{n}{f_s} + \frac{\Delta\phi}{2\pi f_c} \tag{17}$$

where $f_s = 4f_c$ and n is the discrete-time index. The sampling rule in (17) does not effect the constellation rotation at the receiver. On substituting (17) in (16) we get

$$\acute{s}(n) = \Re\left\{\acute{z}(n)\exp\left(i2\pi\frac{f_c}{f_s}n\right)\right\} \tag{18}$$

where

$$\acute{s}(n) = s\left(\frac{n}{f_s} + \frac{\Delta\phi}{2\pi f_c}\right)$$
$$\acute{z}(n) = z\left(\frac{n}{f_s} + \frac{\Delta\phi}{2\pi f_c}\right)\exp\left(i\Delta\phi\right)$$

In reality, $\acute{s}(n)$ is a sampled version of $s(t)$, which in turn consists of the transmitted signal corrupted with impulsive noise. As (18) is the same as (4), the additive noise in $\acute{z}(f_s n/B)$ has independent I and Q components under the AWSαSN framework.

In Fig. 8 we present a schematic that depicts a practical implementation of passband-to-baseband conversion with constellation rotation at the receiver. By setting $f_s = 4f_c$, independent baseband noise components are guaranteed. This

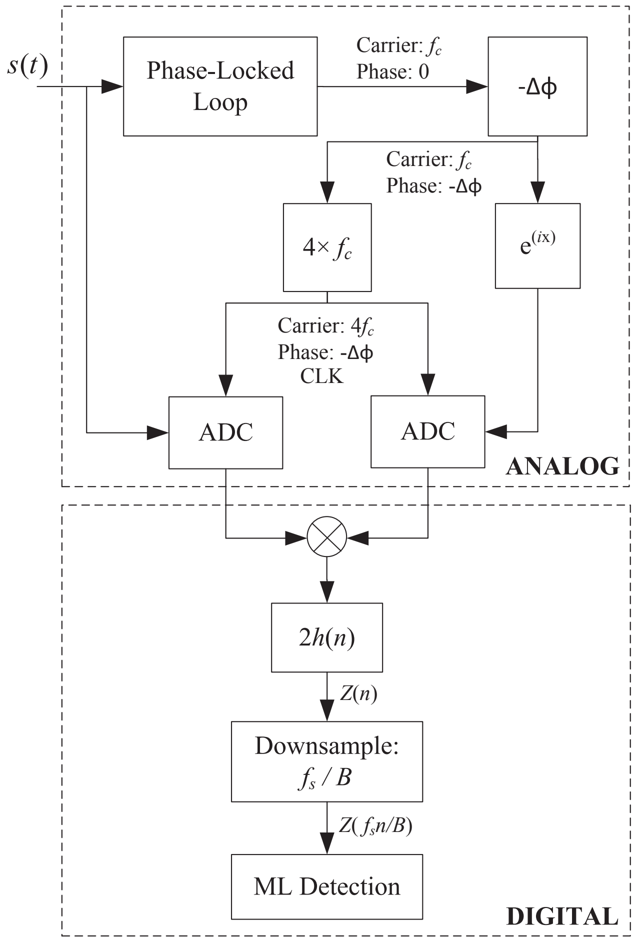

Figure 8: Practical implementation of a single-carrier rotated-constellation scheme.

scheme is applicable for any constellation map that requires rotation while ensuring independence of noise components. The analog and digital blocks of the receiver are also highlighted.

5. CONCLUSION

Ambient noise in shallow waters dominated by snapping shrimp is known to be impulsive and has been modeled accurately by SαS distributions. We examined the structure of complex baseband noise derived from AWSαSN while restricting ourselves to the linear system framework. By changing certain system parameters, different statistical configurations are achieved for the resulting noise. These baseband noise distributions are bivariate SαS and generally anisotropic. With emphasis on the Cauchy case with independent components, it is shown that by efficiently rotating constellation maps the noise anisotropy may be exploited to achieve exceptional error performance in BPSK and QPSK. This advantage can be extended to include other constellation sets as well. Using simulation, we show that error performance trends in the Cauchy case are also encountered in other heavy-tailed SαS cases that correspond to good practical estimates of snapping shrimp noise. We propose an innovative but simple implementation of a single-carrier system that takes advantage of the baseband noise anisotropy by rotating constellations solely at the receiver side while also ensuring independence of noise components. As the analysis provided in this paper is restricted to linear decoders, the provided mechanism can be incorporated within any practical system.

6. REFERENCES

[1] G. Arce. *Nonlinear signal processing: a statistical approach*. Wiley InterScience online books. Wiley-Interscience, 2005.

[2] W. W. L. Au and K. Banks. The acoustics of the snapping shrimp synalpheus parneomeris in kaneohe bay. *The Journal of the Acoustical Society of America*, 103(1):41–47, 1998.

[3] M. Chitre, J. Potter, and S.-H. Ong. Optimal and near-optimal signal detection in snapping shrimp dominated ambient noise. *Oceanic Engineering, IEEE Journal of*, 31(2):497 –503, april 2006.

[4] J. Gonzalez. *Robust techniques for wireless communications in non-Gaussian environments*. University of Delaware, 1997.

[5] J. Gonzalez and G. Arce. Weighted myriad filters: a robust filtering framework derived from alpha-stable distributions. In *Acoustics, Speech, and Signal Processing, 1996. ICASSP-96. Conference Proceedings., 1996 IEEE International Conference on*, volume 5, pages 2833 –2836 vol. 5, may 1996.

[6] J. Gonzalez and G. Arce. Optimality of the myriad filter in practical impulsive-noise environments. *Signal Processing, IEEE Transactions on*, 49(2):438 –441, feb 2001.

[7] J. G. Gonzalez. *Robust techniques for wireless communications in non-gaussian environments*. PhD thesis, University of Delaware, Newark, DE, USA, 1997.

[8] J. G. Gonzalez and G. R. Arce. Statistically-efficient filtering in impulsive environments: weighted myriad filters. *EURASIP J. Appl. Signal Process.*, 2002:4–20, January 2002.

[9] M. W. Johnson, F. A. Everest, and R. W. Young. The role of snapping shrimp (crangon and synalpheus) in the production of underwater noise in the sea. *Biological Bulletin*, 93(2):pp. 122–138, 1947.

[10] A. Mahmood, M. Chitre, and M. A. Armand. PSK communication with passband additive symmetric α-stable noise. *Communications, IEEE Transactions on*, pages 1 –11, 2012 [To Appear].

[11] C. L. Nikias and M. Shao. *Signal processing with Alpha-Stable Distributions and Applications*. Chapman-Hall, New York, 1996.

[12] J. P. Nolan. *Stable Distributions - Models for Heavy Tailed Data*. Birkhauser, Boston, 2012. In progress, Chapter 1 online at academic2.american.edu/$\sim$jpnolan.

[13] A. Papoulis and U. S. Pillai. *Probability, Random Variables and Stochastic Processes*. McGraw-Hill, Boston, Dec. 2001.

[14] J. Proakis. *Digital Communications*. McGraw-Hill, Boston, 4 edition, Aug. 2000.

[15] G. Samorodnitsky and M. S. Taqqu. *Stable Non-Gaussian Random Processes: Stochastic Models with Infinite Variance*. Chapman & Hall, 1994.

[16] M. Versluis, B. Schmitz, A. von der Heydt, and D. Lohse. How snapping shrimp snap: Through cavitating bubbles. *Science*, 289(5487):pp. 2114–2117, 2000.